Structural and Thermodynamic Characterization of a Bioactive Peptide Model of Apolipoprotein E: Side-Chain Lactam Bridges To Constrain the Conformation†

Peizhi Luo,‡ Demetrios T. Braddock,§ Ram M. Subramanian,‖ Stephen C. Meredith,*,‖ and David G. Lynn*,‡

Departments of Chemistry, Biochemistry and Molecular Biology, and Pathology, The University of Chicago, Chicago, Illinois 60637

Received April 7, 1994; Revised Manuscript Received July 29, 1994®

ABSTRACT: Apolipoprotein E plays a critical role in plasma lipoprotein clearance. A peptide model of a highly conserved domain of this protein has been shown to increase low-density lipoprotein binding to fibroblast cell surface receptors. To distinguish between two potential structures—one essentially α-helical and nonamphiphilic, the other an amphiphilic π-helix—synthetic side-chain lactam constraints have been incorporated into model peptides in order to restrict conformational flexibility favoring either the α- or π-helix. Here we provide CD and ^{1}H NMR data suggesting that the more biologically active, putatively α-helical peptide indeed contains two α-helical domains separated by a central bend. Whereas previous studies (Ősapay & Taylor, 1992; Felix et al., 1988) indicated stabilization of α-helices by cross-links between the i and i+4 residues, the current paper demonstrates that cross-links between the i and i+3 residues also stabilize the helix. Indeed, the stabilization afforded by these cross-links is ~1 kcal/mol, similar to that reported for peptides cross-linked between the i and i+4 residues, and derives exclusively from a loss of entropy of the unfolded state. The presence of the α-helical structure appears to correlate well with biological activity. This study provides initial insight into the bioactive structure of this domain of apo E and suggests strategies as to how peptides can be conformationally constrained to enhance their stability and biological function.

Biological peptides (<50 amino acids) can assume an ensemble of conformations in solution. However, as demonstrated by the amphiphilic helical structures of apolipoproteins and many peptide hormones, well-defined conformations are critical for receptor interactions (Kaiser & Kézdy, 1987). Analyses of several peptides and proteins suggested that amphiphilic α-helices (3.6 residues per turn) and possibly also π-helix, (4.4 residues per turn) are secondary structures critical for biological functions (Kasier & Kézdy, 1984a). The π-helices, while first proposed as a potential secondary structure in the 1950s (Pauling & Corey, 1950; Low & Baybutt, 1952; Ramakrishnan & Ramachandran, 1965), has been observed very rarely, at most, in protein structures. Even with marginal stability, however, the π-helix could exist in the amphiphilic form once associated at an interface (Kaiser & Kézdy, 1984a,b; Blanc & Kaiser, 1984). Therefore, these structures may conceivably occur in lipoproteins or at other amphiphilic interfaces (Kaiser & Kézdy, 1984a).

Apolipoprotein E is a ligand for the low-density lipoprotein receptor (LDL-R) (Mahley, 1989; Innerarity et al., 1979) and the LDL receptor related protein (LRP) (Kowal et al., 1989; Hussian et al., 1991; Willnow et al., 1992). The putative receptor binding domain is located at amino acids 140–150 of human apo E (Innerarity et al., 1983; Wilson et al., 1991). The most highly conserved domain, however, is located at amino acids 41–60 (of human apo E) and has no previously assigned function (Braddock et al., 1990; Matsushima et al., 1990). This domain forms separate hydrophilic and lipophilic faces only when arrayed as a π-helix. As an α-helix, the lipophilic amino acids spiral around the surface of the helical cylinder, and this structure is not predicted to be amphiphilic. Recently, we have shown that a synthetic peptide modeling these residues enhances the binding of ^{125}I-LDL to cell surface receptors on normal and LDL receptor deficient human skin fibroblasts, that this peptide normalizes the binding of ^{125}I-LDL from a patient with familial defective apolipoprotein B to fibroblasts, and that these effects are mediated by the LDL-R and LRP (Braddock et al., 1994). Therefore, there is a biological function that can be directly observed with this peptide.

Conservative changes within the peptide made it possible to synthesize amide cross-links between the i and i+3 or the i and i+5 residues at both the N and C termini. It was anticipated that these cyclized amides would stabilize the desired secondary structure, either an α- or a π-helix, respectively. In this paper, we present the detailed characterization of peptide III, a bioactive dicyclic peptide with covalent bridges between i and i+3 residues. We will show that the helix of peptide III is stabilized relative to that of its linear analogue, peptide I, and that this structure contains two helical segments separated by a central bend. The implications for the existence of a π-helix in this peptide are discussed.

MATERIALS AND METHODS

Peptide Synthesis, Purification, and Characterization. A synthetic scheme similar to that developed by Felix et al. (1988) was used to synthesize cross-linked peptides and is reported in full in another paper (Braddock et al., 1994). Briefly, peptides were synthesized by solid-phase methods on a 0.5 mmol scale using an Applied Biosystems (Foster City, CA) Model 431A peptide synthesizer. All amino acids were purchased from Applied Biosystems (ABI, Foster City, CA) except N^{α}-tBoc-Asp-O^{β}-Fmoc and N^{α}-tBoc-Lys-N^{ϵ}-Fmoc,

† Supported by Grant HL-15062 SCOR in Arteriosclerosis (specialized for center research), Grant AHA 89-1020, and NIH Biotechnology Training Grant GM-08369.

* To whom correspondence should be addressed.
‡ Department of Chemistry.
§ Department of Biochemistry and Molecular Biology.
‖ Department of Pathology.

® Abstract published in *Advance ACS Abstracts,* September 15, 1994.

0006-2960/94/0433-12367$04.50/0

which were from Bachem (Torrance, CA) or Peninsula Laboratories Inc. (Belmont, CA). Side chains were cross-linked by utilizing the benzotriazolyl-*N*-oxytris(dimethylamino)phosphonium hexafluorophosphate (BOP) reagent developed by Felix et al. (1988). BOP, 665 mg (1.5 M, 3-fold molar excess), and 2.5 mL of DIEA (approximately 15% of total volume) were introduced through the top of the reaction vessel by pausing the synthesis at the cross-linking point. The reaction vessel top was then replaced, and NMP was added until the vessel was half full (approximately 14 mL). To aid in the eventual removal of peptide chains in which a lactam bridge had failed to form, any unreacted Lys ϵ-amino side-chain groups were coupled to N^{α}-tBoc-*S*-(methylbenzyl)-Cys. After completion of the peptide synthesis, and cleavage of the peptide from the resin, cysteine-containing peptides (i.e., un-cross-linked peptides) were removed from the mixture by reaction with PAM–resin–cysteine beads. The progress of the synthesis was monitored using the quantitative ninhyrin procedure (Sarin et al., 1981). Peptides were cleaved from the resin with HF in an Immuno-Dynamics (La Jolla, CA) HF apparatus, using 10 mL of HF, 1 mL of DMS, 1 mL of anisole, and 0.2 mL of *p*-thiocresol for each gram of resin for 1 h at −3 to −5 °C. Peptides were washed from the resin into 2.5% (w/v) ammonium bicarbonate in water and diethyl ether, the aqueous phase was desalted using Sephadex G-25 chromatography, and the peptides were purified by reverse-phase HPLC using a preparative C-4 Dynamax column (Rainin Instrument Co., Inc., Woburn, MA; 5 μm bead size, 300 Å pore size, 21.4 mm diameter, 250 mm length) in a Waters 600E HPLC (Waters Chromatography Division, Millipore, Inc., Milford, MA). Peptides were eluted using a triethylammonium phosphate aqueous buffer–acetonitrile gradient at approximately 28–32% (v/v) acetonitrile. Peptide purity was assessed on all peptides by amino acid analysis and analytical HPLC. Peptide identity was confirmed by fast atom bombardment mass spectrometry and, in ambiguous cases, amino acid sequencing. Details of these procedures are given in a separate paper (Braddock et al., 1994). By these criteria, peptide products were >99% pure.

CD Spectroscopy. The CD spectra were recorded using a Jasco J-500A spectropolarimeter. Peptides were dissolved in the following solvents: 0.02 M sodium phosphate, pH 7.0 ("low salt"); 0.02 M sodium phosphate, pH 7.0, containing 1.5 M NaCl ("high salt"); or water/trifluoroethanol (TFE) mixtures varying from 0% to 50% (v/v) TFE. To test the effect of ionic strength on helicity in a solvent in which peptides had high helical content, spectra were also measured in 0.02 M sodium phosphate, pH 7.4 in H_2O/TFE, 7/3 (v/v), or 0.02 M sodium phosphate, pH 7.4, 1.5 M NaCl/TFE, 7/3 (v/v). Peptide concentrations were varied between 1 μM and 0.4 mM; concentrations were determined by amino acid analysis (Heinrikson & Meredith, 1984). The measurements were taken using a 1 or 0.1 mm path-length cell, and water-jacketed cells were used when necessary for variable temperature experiments. The spectropolarimeter was calibrated periodically with a standard solution of *d*-camphorsulfonic acid as described previously (Nakagawa et al., 1979).

Thermal Denaturation of Peptides and Thermodynamic Analysis. To compare the stability of peptides I and III, thermal denaturation experiments were performed as follows: peptides were dissolved at 0.1 mM in TFE/H_2O, 1/1 (v/v), in which it had previously been determined that the peptides were helical. The temperature was then increased in increments of 10 °C at a time and allowing at least 1 h for thermal equilibration at each temperature. Equilibration was checked by measuring ellipticity at $\lambda = 222$ nm until a constant ellipticity was attained. Several points were remeasured on the same samples which had been allowed to cool, and in no case was thermal hysteresis observed. The pH was adjusted with either NaOH or HCl after the peptide had been added to the solution. Helical content was calculated by the equation of Greenfield and Fasman (1969); i.e., % helix = $100[([\theta]_{208} + 4000)/-29\,000]$.

The thermodynamic parameters ΔG, ΔH, and ΔS for the unfolding of peptide III and its linear analogue, peptide I, were obtained using a two-state model as a first approximation.

$$\mathrm{H} \overset{K_{\mathrm{unfold}}}{\rightleftharpoons} \mathrm{C}$$

The peptides are assumed to exist in equilibrium between a helical (H) and a "random coil" (C) form, and K_{unfold} is the equilibrium constant for the unfolding reaction.

$$K_{\mathrm{unfold}} = \mathrm{C/H} = (\theta_{\mathrm{exp}} - \theta_{\mathrm{H}})/(\theta_{\mathrm{C}} - \theta_{\mathrm{exp}})$$

In this case, θ_{exp} = experimental molar ellipticity of the peptide solution, and θ_{H} and θ_{C} are the molar ellipticities of the helical and coil forms of the peptide, respectively. Since $\Delta G_{\mathrm{unfold}} = -RT \ln K_{\mathrm{unfold}}$ and $\Delta G = \Delta H - T\Delta S$, it follows from the van't Hoff equation

$$\ln K_{\mathrm{unfold}} = -(\Delta H/RT) + (\Delta S/R)$$

that the enthalpy and entropy of the unfolding reaction can be obtained from a van't Hoff plot of $\ln K_{\mathrm{unfold}}$ vs $1/T$.

NMR Spectroscopy. NMR samples were typically prepared by dissolving 12–15-mg peptides in 400 μL of either 50% (v/v) TFE-d_3 (99% enrichment) with H_2O or D_2O (99.96% enrichment). The samples for both solvents were adjusted to pH 7.0 or 3.0 with additions of HCl or NaOH, and DCl or NaOD in D_2O.

All NMR spectra were recorded on a General Electric Ω500 spectrometer at 20 °C. Hypercomplex quadrature detection (States et al., 1982) was used to obtain pure-phase absorption mode DQF-COSY (Rance et al., 1983) and NOESY (Macura & Ernst, 1980) spectra. Phase-sensitive TOCSY spectra were recorded with use of the Waltz 16 spin-lock pulse to drive the coherence transfer, and a filter was inserted to remove the unwanted coherence transfer pathway by the novel phase cycling procedure which makes recording of the TOCSY spectra fairly routine (Bax & Davis, 1985; Rance et al., 1987). Typical 2D data were collected with 512 FIDs with 2K data points each, 32–96 scans for each FID, a spectral width of 5500–6000 Hz, and 1 s predelay time. For some spectra collected in D_2O, the spectral width was reduced to 2500 Hz in order to resolve the fine structure of cross peaks. The NOESY spectra were collected with different mixing times—150, 200, and 300 ms. TOCSY were collected with several spin-lock times of 30, 60, 80, and 120 ms to achieve direct, single and multiple relayed through-bond magnetization transfer. Solvent suppression was achieved by continuous irradiation or selective excitation at the solvent resonance for spectra collected in H_2O (Sklenar & Bax, 1987). The data were apodized with the Lorentzian–Gaussian or phase-shifted sine-bell function. The first data point in t_1 was multiplied by 0.5 to suppress t_1 ridges (Otting et al., 1986) and also zero-filled in t_1 or symmetrized as necessary.

The $^3J_{\alpha N}$ coupling constants were measured using DQF-COSY spectra recorded in H_2O. Cross sections of cross peaks in the fingerprint region were analyzed and $^3J_{\alpha N}$ extracted using the method of Kim and Prestegard (1989) with increased

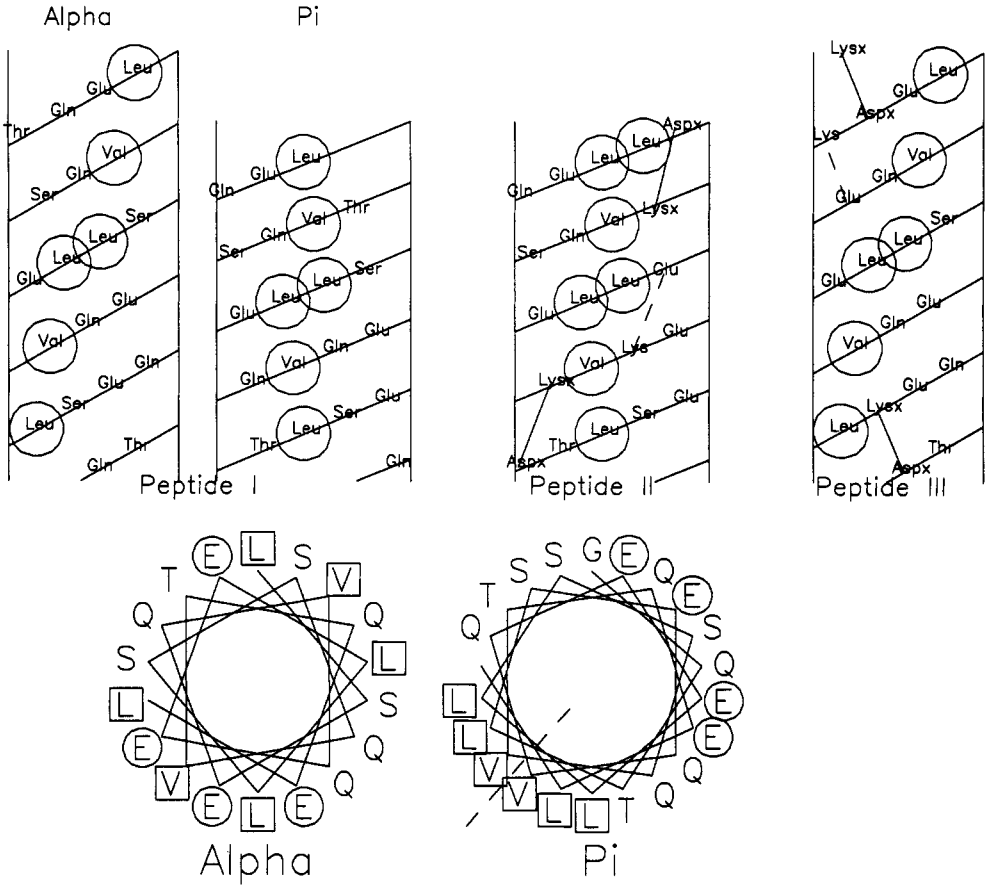

FIGURE 1: Helical net and wheel diagrams. Top row, from left to right: helical net diagrams of peptide I as an α- and a π-helix, peptide II as a π-helix, and peptide III as an α-helix. Lys and Asp residues incorporated into lactam bridges are represented as Lysx and Aspx, respectively, and are connected by solid lines. Hypothesized salt bridges are shown as dotted lines. Lipophilic residues are circled. Bottom row, from left to right: α- and π-helical wheel representations of portions of peptide I. Acidic residues (in this case, all Glu) are in circles; lipophilic amino acids are in squares. A plane of symmetry in the hypothetical π-helix is represented by a dotted line.

digital resolution (32K points) along ω_2. The exchange of labile amide protons was measured on a sample lyophilized from H_2O and redissolved immediately in D_2O. The disappearance of labile protons was monitored at definite time intervals by 1D NMR spectra at 20 °C.

Structure Refinement and Computer Simulation. The NOEs were classified as strong, medium, and weak corresponding to interproton distance constraints of 1.8–2.7, 1.8–3.3, and 1.8–5.0 Å, respectively. The lower bounds for interproton distances were set to the sum of the van der Waals radii of the two protons. The backbone torsional angle constraints were set to ranges of −90° to −10° and −180° to −80° corresponding to $^3J_{\alpha N}$ values of ≤6 and ≥8 Hz. All energy minimization and dynamic simulated annealing calculations (Nilges et al., 1988a,b; Clore et al., 1986a,b, 1990; Kraulis, 1989) were carried out using the Biosym software package with 97 distance and 20 torsional angle constraints. Initial structures were built and modified using InsightII, and force-field parameters were taken from CVFF force fields for all explicit hydrogens. The target function that is minimized during the simulated annealing is comprised of quadratic harmonic terms for covalent geometry, square-well quadratic potentials for the experimental distance restraints, torsion angle restraints, and a quadratic van der Waals repulsion term for the nonbonded contacts. Energy minimization calculations were then carried out on the converged structures using standard energy functions. The bending in the middle of the helix was established from all simulations, and the helices in both ends were refined using loose hydrogen-bond constraints derived from the exchange experiments.

RESULTS

Rationale in the Design and Synthesis of Peptides. In designing peptide models of this domain of human apo E, covalent and salt-bridge cross-links were sought to constrain the peptides to adopt either an α- or a π-helical conformation. Previous investigators have used cross-links or salt bridges between the i and i+4 residues to stabilize helices (Marqusee & Baldwin, 1987; Felix et al., 1988; Ösapay & Taylor, 1990). This spacing, however, is midway between the periodicity of the α-helix (3.6 residues per turn) and the π-helix (4.4 residues per turn). To distinguish between these two structures, therefore, peptides were designed with cross-links between the i and i+3 residues to mimic an α-helix and between the i and i+5 residues to mimic a π-helix. It was not known, however, whether the former cross-links would indeed stabilize an α-helix. Thus, an additional hypothesis to be tested using these designed peptides was that cross-links between the i and i+3 residues would stabilize an α-helical conformation.

Accordingly, the following peptide designs were synthesized:

I. H_2N-GQTLSEQVQEELLSSQVTQELRAG-CO_2H

II. H_2N-GDTLSEKVKEELLESQVKQELLDA-CO_2H

III. H_2N-GDTLKEQVQEELLSEQVKDELKAG-CO_2H

Helical net and wheel diagrams are shown for these structures

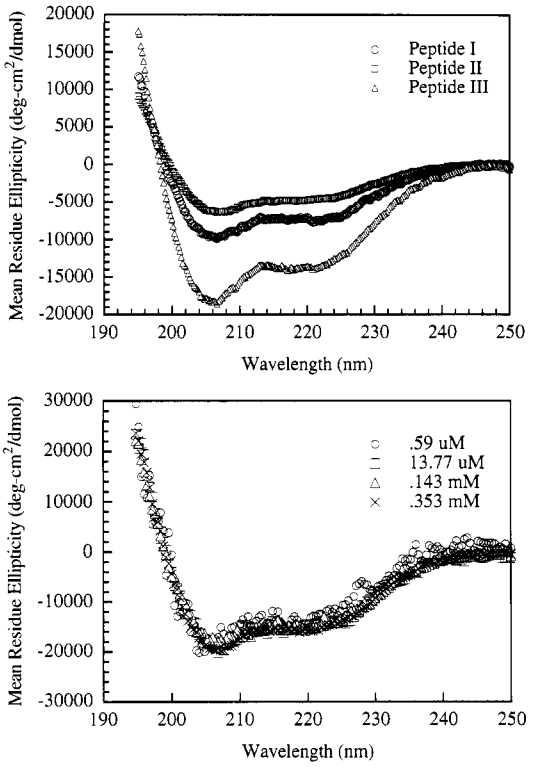

FIGURE 2: CD spectra. Peptides I, II, and III (top panel) were dissolved in 50% (v/v) TFE/H_2O at concentrations of approximately 0.04 mM and CD spectra measured as described in the text. The bottom panel shows mean residue ellipticities for peptide III in 50% (v/v) TFE, at peptide concentrations ranging from 0.59 μM to 0.354 mM. The curves are overlapping, consistent with a lack of self-association. Similar data were obtained for peptides I and II (not shown).

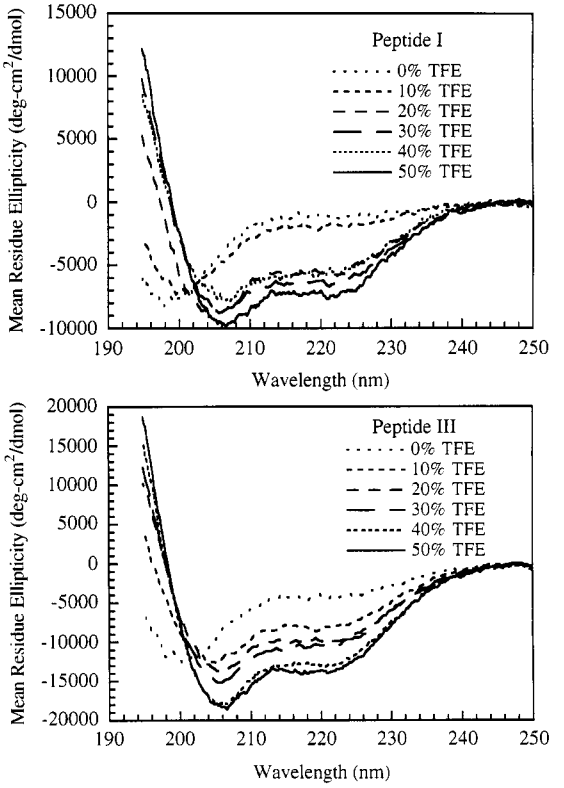

FIGURE 3: Dependence of CD spectra on the TFE concentration. Peptides I (top) and III (bottom) were dissolved in mixtures of water and TFE, varying from 0% to 50% (v/v) TFE at pH 7. The peptide concentration was 0.4 mM and the path length was 0.1 mm.

in Figure 1. Peptide I contains amino acids 41–62 of human apo E with a Gly spacer at each end. The solid lines indicate the positions of lactam cross-links, and the dashed lines represent potential salt bridges. The positions of all lipophilic and acidic residues of peptide I have been conserved in peptide III. The placement of cross-links and salt bridges was chosen wherever possible to replace Gln or Ser, since Gln and Ser resemble the cross-links and salt bridges in being hydrophilic but having no net charge; in addition, Gln has a side-chain amide like that of the cross-link. Peptide II has, at most, weak biological activity in enhancing binding to lipoprotein receptors, and its structure is not further characterized in the present paper.

CD Spectroscopy. The CD spectra of peptides I, II, and III in TFE/H_2O (1/1, v/v) are shown in Figure 2 (top). In aqueous solution, CD spectra of peptide I show little helical content, while peptide III has a helical content of ~20%. The latter level of helicity is similar to that observed for many model amphiphilic α-helical peptides in water when these peptides are in the monomeric state (Yokoyama et al., 1980). Figure 3 (top and bottom) shows that the addition of TFE to the solvent induces the secondary structures for both peptides, with sharp increases in helicity occurring at 20% (v/v) TFE for peptide I and 10% (v/v) TFE for peptide III. As shown in the figures, characteristic negative absorption bands appear at both 208 and 222 nm, and the helical content reaches an apparent maximum at 50% (v/v) TFE. In the NMR and variable temperature CD experiments, the solvent used was 50% (v/v) H_2O or D_2O with TFE-d_3, a structure-inducing solvent which has been used as a mimic of amphiphilic environments (Kaiser & Kézdy, 1984a,b). The CD spectra of peptide III at various temperatures from 0 to 70 °C are shown in Figure 4 (top). The van't Hoff plots for the thermal denaturation curves of peptides I and III (Figure 4, bottom) show two parallel lines with the intercept for peptide III below that of peptide I. From these lines, one calculates that the cross-links stabilize the dicyclic peptide over its linear analogue by 1 kcal mol^{-1} which comes entirely from the loss of entropy of 2.8 cal K^{-1} mol^{-1} (derived from the intercepts of the two lines), with essentially no change in enthalpies of denaturation (derived from the slopes of the two lines). The stabilization energy is in excellent agreement with the results for a peptide stabilized by a Ru(III)-chelated cross-bridge (i to i+4) between peptidyl histidines (Ghadiri & Fernholtz, 1990).

Lack of Self-Association of Peptide III. CD spectra of peptides I, II, and III showed constant molar ellipticity over wide concentration ranges, consistent with nonaggregation of the peptides. Figure 2 (bottom) shows CD spectra for peptide III, the peptide which is characterized by NMR spectroscopy below. As shown in the figure, the mean residue ellipticity for peptide III in 50% TFE (v/v) from λ = 190–250 nm remains unchanged as the peptide concentration varies from 0.59 μM to 0.354 mM. These data indicate that peptide III did not aggregate in this solvent in this concentration range. These data are also consistent with chromatography of the peptide using Sephadex G-25. At peptide concentrations of approximately 20 mg/mL (i.e., approximately 8 mM), the peptide was partially included in the column, consistent only with a monomeric molecular weight.

In order to confirm further that peptide III is monomeric under the experimental conditions to be used for two-dimensional NMR studies, one-dimensional (1D) NMR spectra were collected for peptide III ranging in concentrations from approximately 8 μM to 8 mM at pH 7.0 in 50% TFE (v/v) at 20 °C. The line widths of the amide protons in the 1D NMR spectra were constant at about 12 Hz. The line

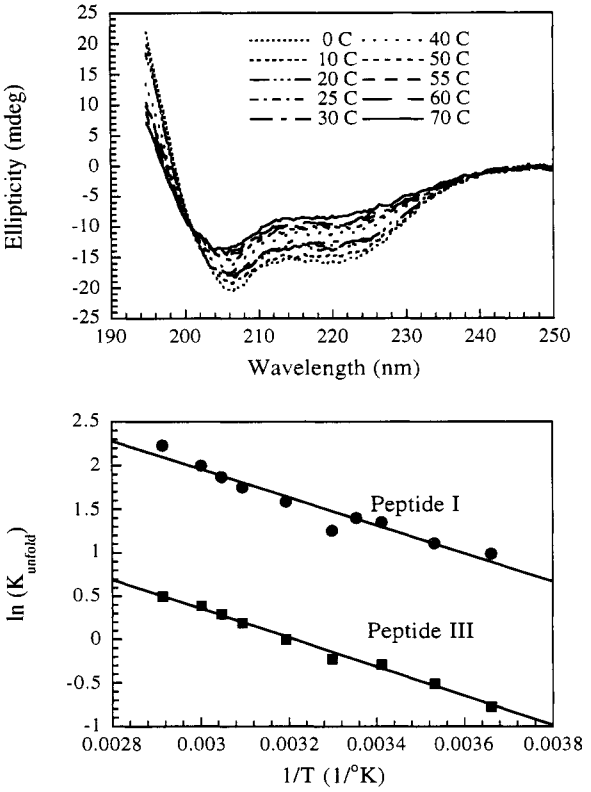

FIGURE 4: Thermal denaturation. Peptides I and III were dissolved in 50% TFE/water (v/v) at 0.1 mM and the CD spectra measured at various temperatures, ranging from 0 to 70 °C, by increments of 10 °C. Absence of thermal hysteresis was confirmed by recooling solutions and remeasuring the CD spectra. The top panel shows the family of curves generated for peptide III; a similar family of curves was obtained for peptide I (data not shown). The bottom panel shows the van't Hoff plots for the thermal denaturation of peptides I and III, calculated as described in Materials and Methods.

shapes and chemical shifts were essentially unchanged. This is in direct contrast with the dramatic changes observed in 1D NMR spectra observed when amphiphilic peptides self-associate (Ciesla et al., 1991; Osterhout et al., 1992). Taken together, these data indicate that peptide III does not self-associate even at the high concentrations used for NMR experiments.

Resonance Assignments and Spin System Identification. Complete assignments of proton resonance for peptide III were obtained using the standard assignment strategy of Wüthrich (1986). The amino acid spin systems were identified by the through-bond coupling network of the DQF-COSY and TOCSY experiments collected in 50% (v/v) D_2O or H_2O with TFE-d_3. The sequence-specific assignments of amino acid spin systems were further achieved by through-space sequential connectivities of the NOESY experiment in 50% (v/v) H_2O with TFE-d_3. Ambiguities in the assignments caused by peak overlap were further resolved by comparing the above spectra at pH 7.0 and 3.0, since differences in the chemical shift position for certain residues were observed at two pH values. Figure 5 shows the fingerprint region of the DQF-COSY spectrum that consists of the cross peaks between $C_\alpha H$ and amide protons at pH 7.0. Twenty-two NH–$C_\alpha H$ cross peaks out of 24 amino acid residues were identified in addition to the two ϵ-amide proton cross peaks with the ϵ-side-chain protons from the lactam bridges. As shown in Figure 6, the TOCSY spectra resolved the intraresidue spin systems of 22 amino acids, including Asp19, which was not identified in DQF-COSY. Different spin-lock times were used to achieve multiple through-bond magnetization transfer for all amino

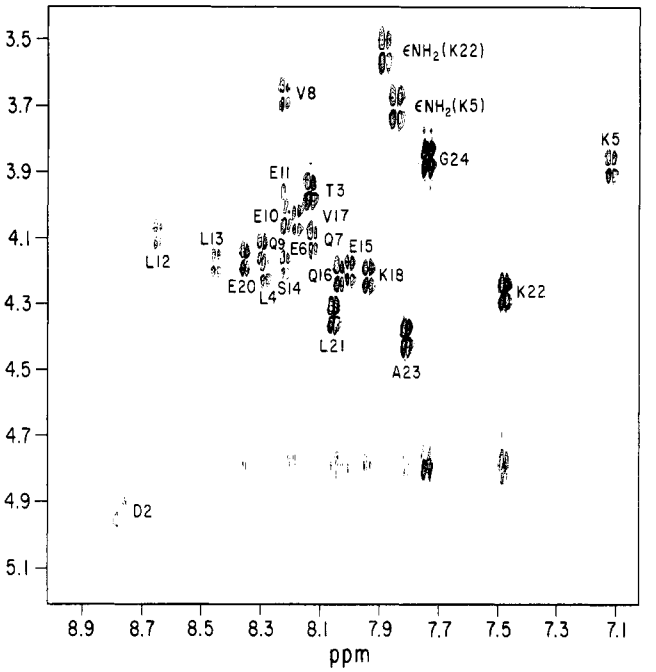

FIGURE 5: $C_\alpha H$–NH fingerprint region of the DQF-COSY spectrum. Peptide III was dissolved in 1:1 (v/v) TFE-d_3/H_2O at pH 7, and the spectra were acquired at 20 °C. The cross peaks are annotated by standard one-letter symbols for the amino acids and the residue number in the sequence.

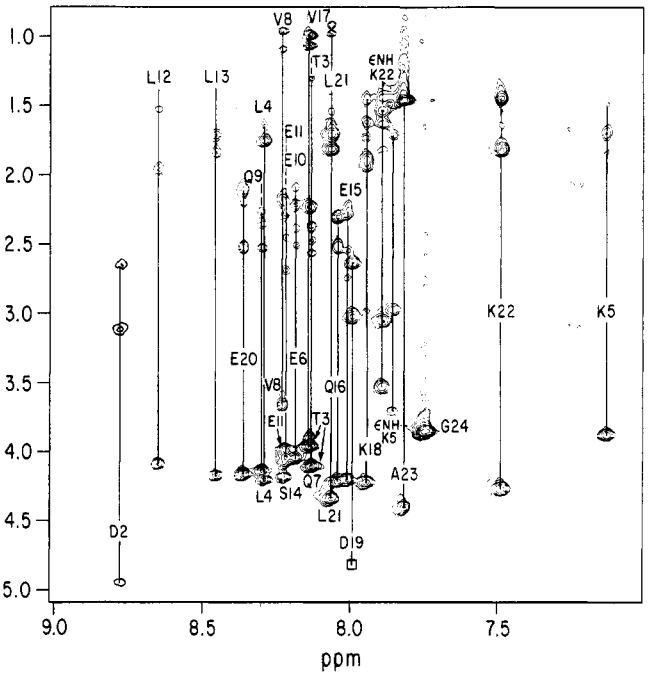

FIGURE 6: Amide to aliphatic region of the TOCSY spectrum. Peptide III was dissolved in 1:1 (v/v) TFE-d_3/H_2O at pH 7, and the spectra were acquired at 20 °C, using an 80 ms spin-lock time for the TOCSY experiment. Each intraresidue spin system is connected by a solid line and annotated as in Figure 5.

acids except for leucines, for which the $C_\alpha H$ to methyl connectivities were further established by spectra collected in D_2O (data not shown). The well-resolved spin systems for aspartic acids in D_2O provided enough confidence to recover the missing connectivities in NOESY experiments in H_2O using selective excitation. Almost one-third of the amino acids in the peptide are Glu and Gln residues in close proximity in the sequence; again the severe chemical shift dispersion problem was resolved by comparing spectra collected at pH 7.0 and 3.0. Figure 9 shows the fingerprint region of the

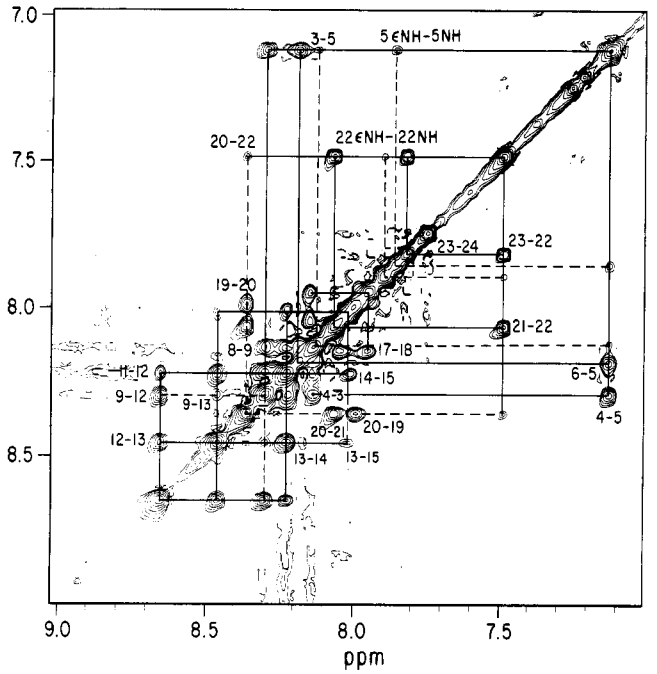

FIGURE 7: NH–NH region of a NOESY spectrum. Peptide III was dissolved as in Figure 5, and the data shown are for a 300-ms mixing time. Sequential $d_{NN}(i, i+1)$ NOE connectivities are indicated by sequence numbers of the pair of adjacent residues (connected with solid lines). Dashed lines are used to indicate cross peaks between Q9–L12, Q9–L13, T3–K5, E20–K22, $N_\epsilon H$ (K5)–NH (K5), and $N_\epsilon H$ (K22)–NH (K22).

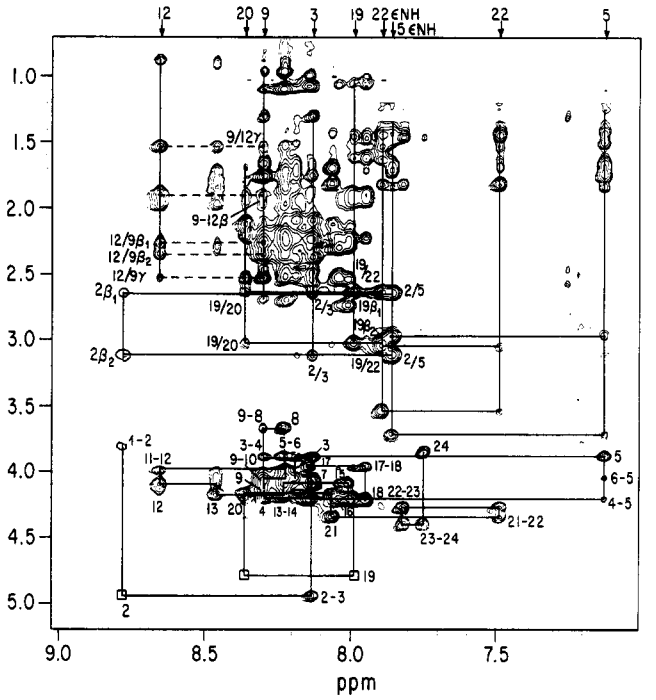

FIGURE 8: NH to $C_\alpha H$ and aliphatic side-chain region of a NOESY spectrum. Peptide III was dissolved and analyzed as in Figure 7 with a mixing time of 300 ms. Sequential $d_{\alpha N}(i, i+1)$ NOE connectivities are indicated by sequence numbers of the pair of adjacent residues (connected with solid lines). Lactam bridges and the bend region in the middle of the peptide are connected by solid lines. Amide protons to side-chain connectivities indicative of the bending contacts for Q9 and L12 are highlighted with dashed lines: NH (L12)–$C_\beta H$, $C_\gamma H$ (Q9) and NH (Q9)–$C_\beta H$ (L12).

TOCSY spectrum at pH 3.0 and the appearance of an additional amide proton resonance for the K18 which will be discussed in detail below. The pH titration does change the chemical shift overlap for Glu residues, as expected, a fact which aids in the sequential assignments.

Sequence-Specific Assignments. Sequential assignments of the identified spin systems were obtained by linking the NOE connectivities using the NN ($i, i+1$) (Figure 7), αN ($i, i+1$), and βN ($i, i+1$) (Figure 8) cross peaks in the NOESY spectra in H_2O at pH 7.0. The assignments at pH 3.0 (Figures 10 and 11) confirmed some of the most important structural features observed at pH 7.0. The strong amide–amide proton cross peak between Q9 and L12 is complicated by the overlap of amide protons of L4 and Q9 at pH 7.0, but the same strong cross peak appears again at pH 3.0 at which the amide proton of Q9 is well separated from others. The complete assignments of peptide III at pH 7.0 and 3.0 are summarized in Tables 1 and 2 together with the coupling constants between amide and Cα protons. Figure 12 summarizes the NOE connectivities observed at pH 7.0 and 3.0.

NMR Characterization of Lactam Bridges. Several characteristics NMR features of lactam bridges have been observed (Felix et al., 1988; Fry et al., 1992) that were consistent with these results. The backbone amides of the bridging K5 and K22 are upfield shifted to a region well separated from other amides indicative of the cyclized amides. The ϵ-protons of Lys and β-protons of Asp in the lactam bridges are well resolved and downfield shifted, further supporting the presence of the cyclic amide (Figures 6 and 8). The amide protons of the side chain are strongly coupled with the ϵ-protons of the Lys in the ring, and the Lys backbone amide protons are coupled with other side-chain protons as seen in the TOCSY experiment (Figure 6). Both side-chain and backbone amide protons for the cross-linked lysines show cross peaks

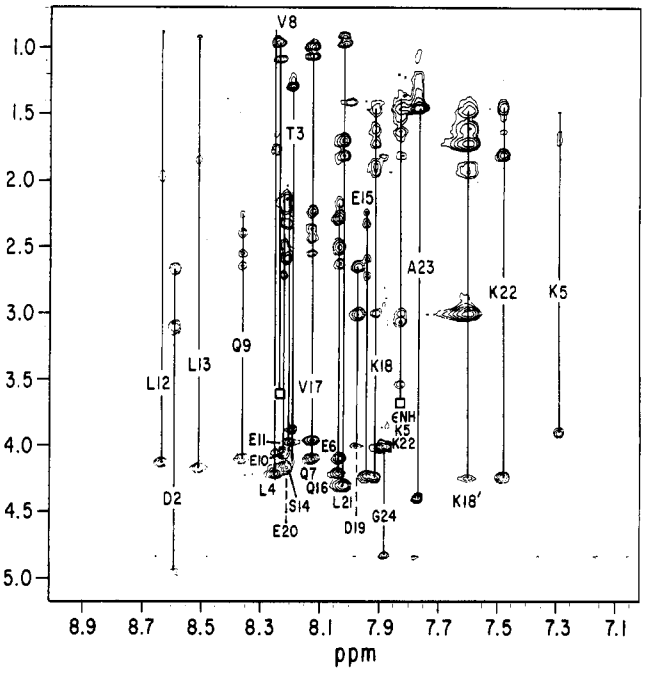

FIGURE 9: Amide to aliphatic region of the TOCSY spectrum. Peptide III was dissolved and analyzed as in Figure 6 but with a spin-lock time of 120 ms at pH 3. Each intraresidue spin system is connected by a solid line and annotated as in Figure 5. Note that the amide of Q9 is well separated from other residues and there are two chemical shifts assigned for K18.

with their own side-chain protons, and the side-chain amide protons also display strong cross peaks with the β-protons of aspartates in the lactam rings (Figure 8). The NOEs (highlighted by the dashed lines in Figure 7) between the side-chain and the backbone amide protons are also observed

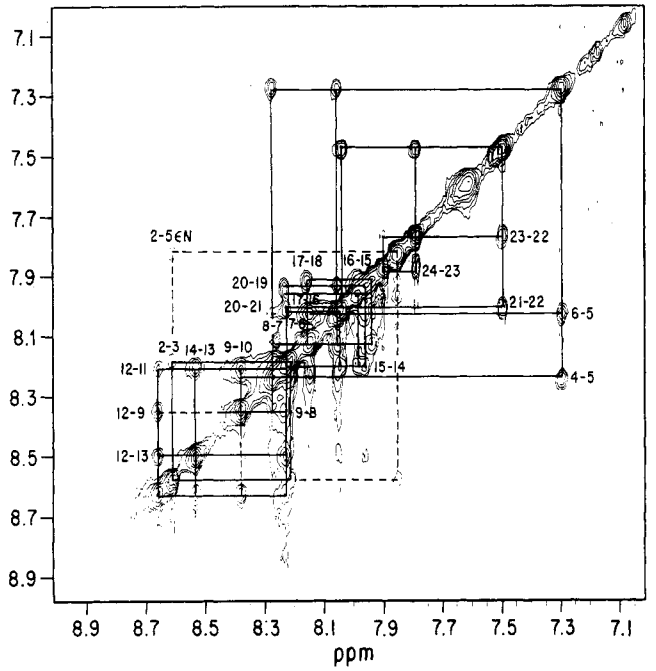

FIGURE 10: NH–NH region of a NOESY spectrum. Peptide III was dissolved and analyzed as in Figure 7, with a mixing time of 300 ms but at pH 3.0. Sequential $d_{NN}(i, i+1)$ NOE connectivities are indicated by sequence numbers of the pair of adjacent residues (connected with solid lines). The amide–amide cross peaks of Q9–L12 are connected by dashed lines.

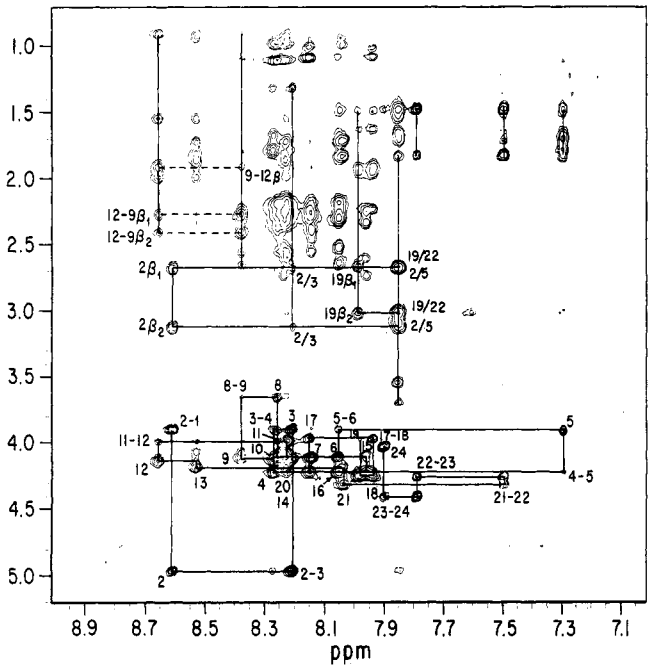

FIGURE 11: NH to $C_\alpha H$ and aliphatic side-chain region of a NOESY spectrum. Peptide III was dissolved and analyzed as in Figure 10, with a mixing time of 300 ms at pH 3. Sequential $d_{\alpha N}(i, i+1)$ NOE connectivities are indicated by sequence numbers of the pair of adjacent residues (connected with solid lines). Lactam bridges and the bend region in the middle of the peptide are connected by solid lines. Amide protons to side-chain connectivities for Q9 and L12 are highlighted with dashed lines: NH (L12)–$C_\beta H$, $C_\gamma H$ (Q9) and NH (Q9)–$C_\beta H$ (L12).

at pH 7.0, which indicated that the side-chain amide protons are proximal to the backbone amides and possibly hydrogen-bonded with the carbonyl group of the backbone. Another feature observed is the cross peaks of $NN(i, i+2)$ and $\alpha N(i, i+2)$ which are highlighted in Figure 7 by the dashed lines

Table 1: Chemical Shift Assignments and $^3J_{\alpha N}$ Coupling Constants for Peptide III at pH 7 in 50% (v/v) Aqueous TFE at 20 °C

residue	NH	$C_\alpha H$	$C_\beta H$	$C_\gamma H$	$C_\delta H$	$C_\epsilon H$; $N_\epsilon H$	$^3J_{\alpha N}$ (Hz)
G1		3.82					
D2	8.76	4.95	2.67, 3.12				8.99
T3	8.12	3.97	4.11	1.32			
L4	8.28	4.22	1.76, 1.76	1.68	0.96, 1.00		5.1
K5	7.11	3.89	1.76, 1.85	1.40, 1.50	1.70, 1.70	3.72, 3.98; 7.85	5.8
E6	8.17	4.06	2.10, 2.21	2.39, 2.52			5.5
Q7	8.12	4.12	2.22, 2.38	2.48, 2.57			5.8
V8	8.21	3.67	2.20	0.95, 1.10			5.9
Q9	8.29	4.14	2.28, 2.36	2.52, 2.52			5.9
E10	8.20	4.05	2.20, 2.28	2.48, 2.69			6.2
E11	8.21	4.00	2.20, 2.28	2.48, 2.69			4.3
L12	8.64	4.10	1.97, 1.97	1.52	0.88, 0.88		5.9
L13	8.45	4.19	1.85, 1.85	1.72	0.92, 0.92		6.1
S14	8.21	4.20	4.06, 4.09				4.3
E15	8.02	4.22	2.25, 2.28	2.55, 2.75			5.2
Q16	8.04	4.22	2.30, 2.30	2.54, 2.54			5.4
V17	8.15	3.98	2.25	1.02, 1.08			
K18	7.93	4.22	1.80, 1.80	1.45, 1.45	1.64, 1.74	2.88, 2.88	5.6
D19	8.00	4.80	2.64, 3.02				
E20	8.35	4.17	2.12, 2.20	2.52, 2.52			
L21	8.05	4.34	1.72, 1.83	1.72	0.95, 1.00		5.9
K22	7.47	4.27	1.85, 1.85	1.46, 1.46	1.55, 1.65	3.06, 3.55; 7.80	5.9
A23	7.80	4.41	1.48				6.9
G24	7.73	3.87					10.7

Table 2: Chemical Shift Assignments and $^3J_{\alpha N}$ Coupling Constants for Peptide III at pH 3 in 50% (v/v) Aqueous TFE at 20 °C

residue	NH	$C_\alpha H$	$C_\beta H$	$C_\gamma H$	$C_\delta H$	$C_\epsilon H$; $N_\epsilon H$	$^3J_{\alpha N}$ (Hz)
G1		3.91					
D2	8.60	4.96	2.67, 3.11				4.3
T3	8.19	3.90	4.18	1.30			4.5
L4	8.26	4.20	1.65, 1.74	1.74	0.98, 1.12		5.1
K5	7.28	3.90	1.71, 1.85	1.50, 1.50	1.70, 1.70	2.99, 3.66; 7.84	5.5
E6	8.03	4.11	2.18, 2.27	2.50, 2.62			5.3
Q7	8.12	4.12	2.23, 2.37	2.44, 2.55			7.1
V8	8.24	3.66	2.17	0.96, 1.08			7.2
Q9	8.36	4.11	2.26, 2.39	2.54, 2.63			
E10	8.23	4.06	2.18, 2.32	2.47, 2.72			5.9
E11	8.20	3.99	2.15, 2.21	2.32, 2.58			5.5
L12	8.64	4.14	1.53, 1.92	1.97	0.90, 0.90		5.5
L13	8.51	4.19	1.70, 1.85	1.85	0.93, 0.93		5.8
S14	8.25	4.18	4.00, 4.10				
E15	7.95	4.22	2.24, 2.32	2.60, 2.72			5.7
Q16	8.03	4.21	2.18, 2.27	2.50, 2.62			5.8
V17	8.13	3.97	2.23	1.02, 1.09			5.8
K18	7.92	4.25	1.90, 1.90	1.46, 1.46	1.62, 1.62	3.00, 3.00	6.2
K18′	7.60	4.25	1.90, 1.90	1.46, 1.46	1.62, 1.62	3.00, 3.00	
D19	7.99	4.02	2.65, 3.02				
E20	8.22	4.14	2.15, 2.21	2.58, 2.58			
L21	8.02	4.31	1.71, 1.81	1.71	0.92, 0.98		6.3
K22	7.48	4.25	1.81, 1.81	1.50, 1.50	1.74, 1.74	3.08, 3.54; 7.84	6.9
A23	7.77	4.41	1.46				5.2
G24	7.89	4.03	4.81				9.8

and Figure 12a at pH 7.0 for both cross-linked regions. The NOE connectivity pattern and exchange rate for G24, A23, and K22 suggested that fraying at the end of the helix is slight, which means that the lactam bridge stabilizes a portion of the helix extending beyond the lactam ring.

Presence of a Central Bend Domain. The amide–amide cross peak of Q9 with L12 and a weak one with L13 (highlighted by the dashed lines in Figure 7) suggest the presence of an unusual bend in the middle of the peptide. The occurrence of this bend is further supported by the NOEs of

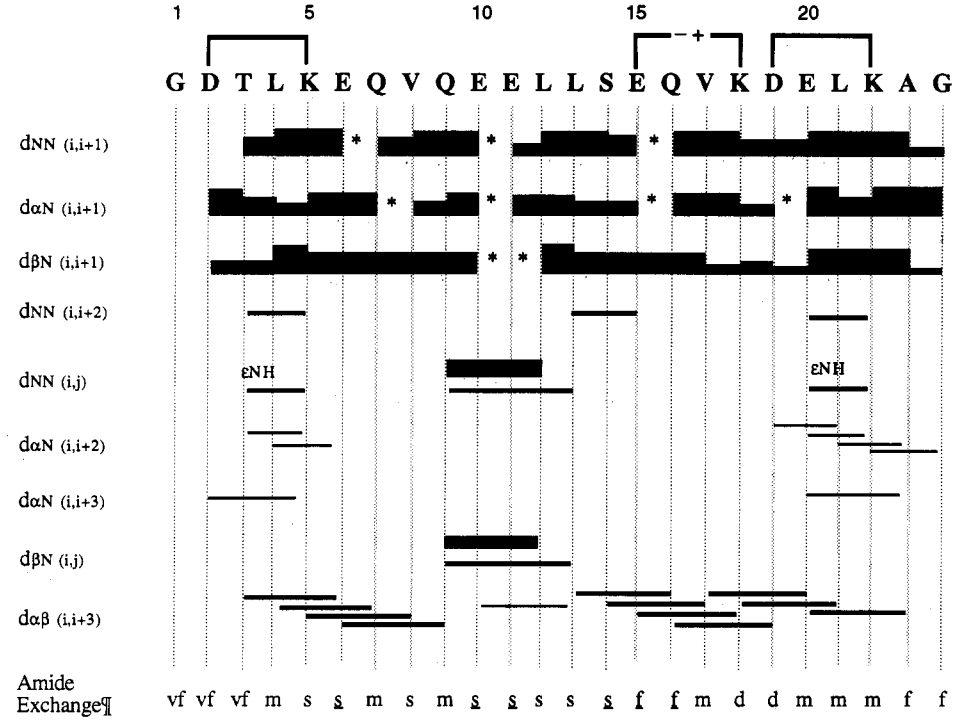

¶ Relative rate of wash out with D_2O: vf, < 5 min. ; f, 15 to 30 min. ; m, 30 to 180 min. ; s, > 240 min.

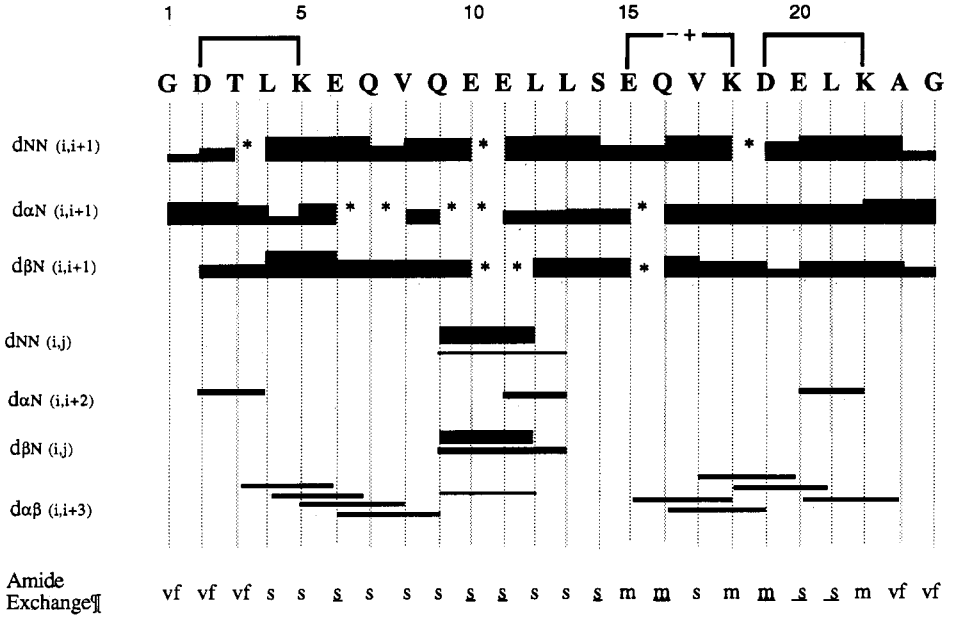

¶ Relative rate of wash out with D_2O: vf, < 7 min. ; m, 30 to 240 min. ; s, > 240 min.

FIGURE 12: Summary of NOE connectivities. Peptide III NOEs at pH 7 (top) and 3 (bottom). Thick solid lines indicate unambiguous NOEs with the varying heights representing qualitatively the relative intensity of the cross peaks. Asterisks (*) indicate overlapping or missing cross peaks. Relative exchange rates of amide protons are monitored after the sample is dissolved in D_2O; underlines indicate possible ambiguity due to resonance overlap.

the amide NH of Q9 with $C_\beta H$ and $C_\gamma H$ of L12 and the amide NH of L12 with $C_\beta H$ and $C_\gamma H$ of Q9 (highlighted by the dashed lines in Figure 8). At pH 3.0, the amide NH of Q9 is well separated from other residues (Figure 9), which eliminates ambiguities due to the chemical shift overlap of amide protons of L4 and Q9 at pH 7.0. Again a strong amide–amide cross peak is observed, and the NOEs between their amide protons with the respective side-chain protons are detected (Figures 10 and 11, dashed lines) for Q9 and L12 at pH 3.0. A similar backbone bend has been reported in a recent paper of an N-capped peptide (Lyu et al., 1993). An unusual feature of the bend in peptide III, in addition to the strong NOE cross peak, is the very slow backbone amide proton exchange rate for V8, Q9, L12, and L13. Although, *a priori*, self-association would be a reasonable explanation of this slow exchange, such an explanation is not consistent with the data presented above that peptide III does not self-associate. Comparison of the data with those of Wüthrich (1986) indicate that the proposed bend in peptide III does not fit into any classical pattern for bends.

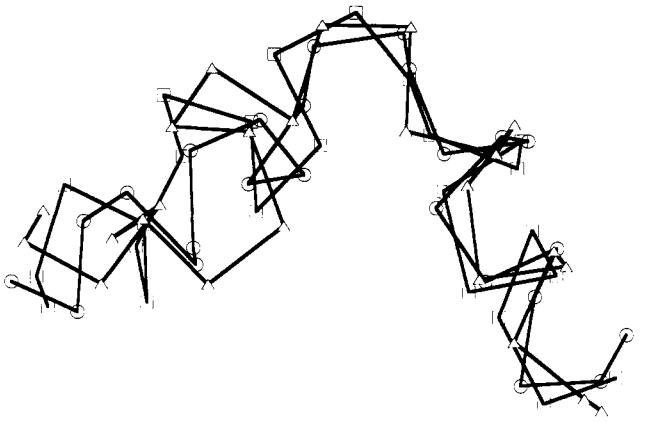

FIGURE 13: Superposition of structures generated from dynamic simulated annealing calculations with NMR constraints. Three structures from ten independent dynamic simulated annealing calculations starting from random coordinates of atoms were superimposed using Cα traces. The potential H-bonding in α-helices identified from exchange data was incorporated into the structure using a range of potential H-bond distances compatible with either an α- or a 3_{10}-helix: N–O, 2.8–4.2 Å; H–O, 1.8–3.2 Å. Note that the structures all contain the helix–bend–helix structural motif.

pH-Induced Changes at the Salt Bridge. By altering the pH, ambiguities due to overlap of the chemical shifts were resolved, and additional structural features of the peptide were established. Chemical shifts at both 7.92 and 7.60 ppm were observed for the amide proton of K18 at pH 3.0 (Figure 9). A potential salt bridge between E15 and K18 was incorporated into the design of the peptide. The Glu side-chain carboxylate is expected to be partially protonated at pH 3.0, breaking the salt bridge, and indeed, a second conformation for K18 is observed (7.60 ppm for the K18 amide) which exchanges slowly on the NMR time scale. At pH 7, where the salt bridge should be strong, the chemical shift for the K18 NH occurs at 7.93 ppm. Few other changes were observed in the NMR spectra as a function of the pH change, suggesting that the salt bridge contributes little to the overall stabilization of the secondary structure. CD measurements in the presence of high and low salt were consistent with this assertion, showing no change in the helical content of the peptide in both H_2O and 30% TFE (v/v) (data not shown).

Structural Model Generated from Dynamic Simulated Annealing Calculations with NMR Constraints. Dynamic simulated annealing protocols were used to search the conformational space of the peptide with distance and dihedral angle constraints. Three structures from ten independent calculations started from random coordinates of atoms were overlaid using Cα traces (Figure 13). The derived structures showed good agreement with the constraints, having no distance violations greater than 0.3 Å and torsional angle violations greater than 5°. Even though the RMSD among these structures are large (about 3.5 Å for Cα traces), the topological similarities are satisfactory in terms of the extensive conformational sampling for a short peptide without tertiary constraints (Clore et al., 1986a,b; Billeter et al., 1987). As shown in the figure, all three traces show a helix–bend–helix structural motif. Figure 14 shows the structural model of peptide III. The model shows two helices (purple ribbons), separated by a bend in the middle of the peptide (yellow ribbon). The two lactam bridges are shown within the helices at both ends; the amide protons of the side chains sit inside the rings formed by the lactams (white balls).

DISCUSSION

Successful constraints of secondary structural elements in model peptides have been possible with salt bridges (Marqusee & Baldwin, 1987), disulfide bonds (Oas & Kim, 1988; Pease et al., 1990; Jackson et al., 1991), metal chelators (Ruan et al., 1990; Ghadiri et al., 1990), and side-chain amide linkages (Felix et al., 1988; Ösapay & Taylor, 1990). The lactam bridge possesses distinct advantages as a cross-linking strategy including ease of synthesis with high yields using existing solid-phase syntheses (Felix et al., 1988; Braddock et al., 1994), resistance to proteolysis, and insensitivity to the redox conditions in biological media.

Other investigations have suggested that cross bridges between the *i* and *i*+3 residues do not significantly stabilize the α-helix (Marqusee & Baldwin, 1987; Felix et al., 1988). However, the data presented on peptide III establish that Asp^{i} to Lys^{i+3} lactam bridges stabilize the α-helical conformation for the residues spanned by the ring. In particular, there is a notable lack of fraying of the helix at the termini which are adjacent to the cross-links. The NMR spectra do suggest slight local distortion of the helix in the immediate vicinity of the cross-links, suggesting some 3_{10}-helix character, raising the possibility of enforcing one or another helical periodicity using the lactam bridges with different spacing between residues. The pH dependence of the NMR data also supports the existence of a salt bridge between E15 and K18, i.e., between the *i* and *i*+3 residues. Both NMR and CD data suggest that the salt bridge has little effect on the stability of the secondary structure.

The NMR data also indicate that Q9 and L12 are spatially proximal to one another, specifying a bend in this domain. The backbone amide exchange rate in this region is quite slow, suggesting a structure in which these protons are protected from solvent, but at this point it is not obvious that the residues exist in a classical turn (Wüthrich, 1986). During the course of this work, the crystal structure of a portion of apo E containing this region was solved (Wilson et al., 1992). In the X-ray structure, the domain containing residues 41–60 is comprised of parts of helices H1 and H2, all of the short connecting helix, Hc (residues 44 to 53), and the turns between these helices. If the folding of peptide III were identical to that of the crystal, then two bends would have been observed: the first starting at K5 in peptide III (corresponding to S44 in apo E) and the second starting at S14 (S53 in apo E). The replacement of S5 by K5 in peptide III in order to form the helix-stabilizing lactam bridge may overcome the signal for a turn in apo E. On the other hand, the bend observed between Q9 and L12 and/or L13 is shifted by only one residue and is roughly consistent with the expectation from the X-ray structure. Thus, the latter structure consists of a helix–turn–helix structural motif which is topologically similar to that observed in the X-ray structure. The conservation of the observed topological structure under quite different conditions and the 3–5-fold enhancement of a biological activity resulting from a 1 kcal/mol stabilization of the helical content both suggest that peptide III resembles apo E in its bioactive conformation.

As mentioned above, analysis of the amino acid sequence of apo E (Finer-Moore & Stroud, 1984) suggested that amino acids 41–60 might form an amphiphilic π-helix; i.e., the periodicity of lipophilic amino acids was 4.5, close to the periodicity of the π-helix (4.4 amino acids per turn). Biological and structural studies of apo E suggest the existence of at least two and possible more distinct and stable structures. Kowal et al. (1990) demonstrated a difference between

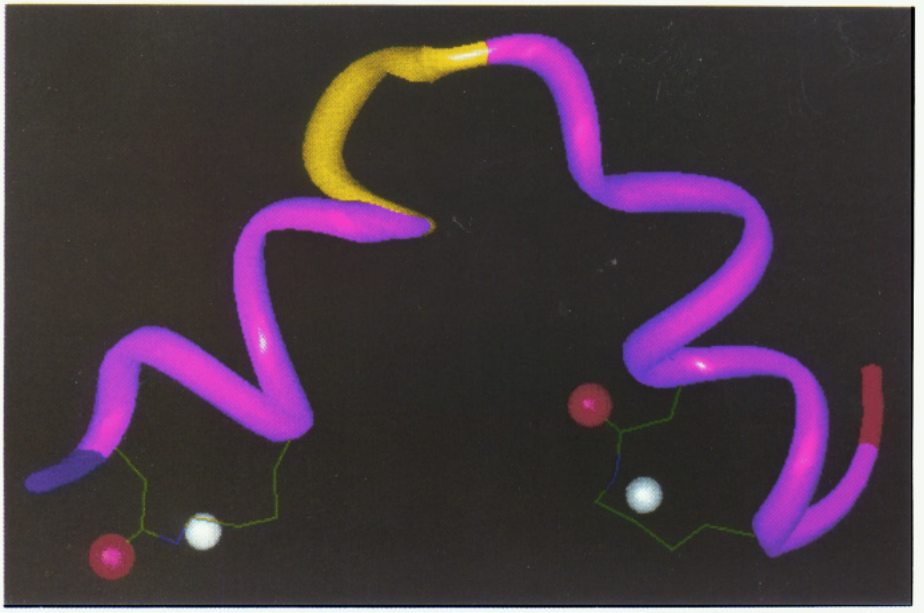

FIGURE 14: Computer-generated model. A ribbon diagram connecting the α-carbons of peptide III; the N-terminus is blue, the C-terminus is red, and the bend region is shown in yellow. The lactam cross-links are shown with a white ball as the amide proton connected with a red ball as the amide oxygen atom. The positions of the other side-chain atoms were not restrained or computed.

endogenous apo E (in β-VLDL) and exogenous apo E (added to β-VLDL) in that only the latter elicited binding of β-VLDL to the LRP; the authors hypothesize that two distinct conformations of apo E exist, only one of which is active. It is not known how closely any of these hypothetical structures resemble the crystal structure. Furthermore, it is not known whether the structure observed in the crystal is best considered as an "active" or "inactive" form of apo E, since the delipidated protein (similar to the crystallized fragment) binds to the LDL receptor with only $^1/_{500}$th of the affinity of the lipidated form. Whether any of these hypothetical structures contain a π-helix is not known.

The two helical segments in peptide III are interrupted by a prominent bend, and it is important to understand the energetic reasons enforcing the turn. Two distinct possible reasons present themselves, both of which may be operative in this peptide. First, it has been proposed (Presta & Rose, 1988; Richardson & Richardson, 1988; Stickle et al., 1992; Harper & Rose, 1993) that certain consensus sequences "end-cap" α-helices, either by "N-capping" (Serrano & Fersht, 1989; Bell et al., 1992; Serrano et al., 1992; Lyu et al., 1993) or by "C-capping" (Kim & Baldwin, 1984; Presta & Rose, 1988; Zhou et al., 1994) the helix, accounting for the short length (average of 12 residues) of α-helices in proteins and isolated peptides. The bend in peptide III could be rationalized if the helical boundary conditions exist for two terminal helices. The N-terminal helix in peptide III is consistent with C-capping: Q9 is one of the preferred amino acids at the C-cap position which terminates helical propagation by H-bonding with the carbonyl oxygen of K5 and possibly E6 (Zhou et al., 1994). The second helix in peptide III starts with the highly preferred S14 in an N-cap position (Harper & Rose, 1993; Lyu et al., 1993) which initiates the helical structure, even though the N3 site is V17, precluding a prominent cyclic hydrogen-bonded SXXE "N-capping box". Nevertheless, it has been shown that an α-helix with T at the N-cap site but G at the N3 site acts as an N-cap to stabilize an α-helix (Serrano & Fersht, 1989).

Second, the bend, as shown in Figure 13, would place the lipophilic side chains in a pocket, somewhat shielded from the aqueous medium. It is not yet known the extent to which the two helices associate, but it is possible that in the peptide, as with the crystal, the bend is stabilized through a hydrophobic effect. The exposure of the lipophilic amino acid side chains to the surrounding aqueous medium would be minimized through the formation of a helical bundle with a lipophilic interior. Westerlund and Weisgraber (1993) have demonstrated that such a helical bundle in apo E can open and spread onto an amphiphilic interface (e.g., phospholipid/water or air/water interfaces), with reorientation of lipophilic side chains toward the nonaqueous phase. Such a conformational shift may reflect the occurrence of a "switch" sequence in apo E, such has been found in certain viral coat proteins (Reed & Kinzel, 1991, 1993), and may conceivably be involved in the switch from bioinactive to bioactive forms of apolipoprotein E. It is possible that an inherently unstable or marginally stable structure, such as an amphiphilic π-helix or a helix–turn–helix motif, might form transiently and then reorient in such a way as to shield lipophilic side chains from the aqueous medium. Further elucidation of the structural determinants of this portion of apo E may shed more light on this model for ligand–receptor interactions and may prove of practical value in developing strategies to enhance the clearance of atherogenic lipoproteins from circulation.

ACKNOWLEDGMENT

We thank Dr. Dean Astumian for the generous use of computing facilities and John Leitzel for stimulating discussion. We also thank Dr. Clyde Hutchinson for instruction in spin dynamics and Dr. Arthur Bates for technical assistance in NMR.

REFERENCES

Bax, A., & Davis, D. G. (1985) *J. Magn. Reson. 65*, 355–360.
Bell, J. A., Becktel, W. J., Sauer, U., Baase, W. A., & Matthews, B. W. (1992) *Biochemistry 31*, 3590–3596.
Billeter, M., Havel, T. F., & Wüthrich, K. (1987) *J. Comput. Chem. 8*, 132–141.
Blanc, J. P., & Kaiser, E. T. (1984) *J. Biol. Chem. 259*, 9549–9556.
Braddock, D. T., Kovatsits, P. G., & Meredith, S. C. (1990) in *Molecular Biology of Atherosclerosis* (Attie, A. D., Ed.) Elsevier Science Publishing Co., Inc., New York.

Braddock, D. T., Mercurius, K., Davies, P. F., & Meredith, S. C. (1994) (submitted for publication).
Ciesla, D. J., Gilbert, D. E., & Feigon, J. (1991) *J. Am. Chem. Soc. 113*, 3957–3961.
Clore, G. M., Martin, S. R., & Gronenborn, A. M. (1986a) *J. Mol. Biol. 191*, 553–561.
Clore, G. M., Nilges, M., Sukumaran, D. K., Brünger, A. T., Karplus, M., & Gronenborn, A. M. (1986b) *EMBO J. 5*, 2729–2735.
Clore, G. M., Appella, E., Yamada, M., Mutsushima, K., & Gronenborn, A. M. (1990) *Biochemistry 29*, 1689–1696.
Felix, A. M., Wang, C.-T., Heimer, E. P., & Fournier, A. (1988) *Int. J. Pept. Protein Res. 31*, 231–238.
Finer-Moore, J., & Stroud, R. (1984) *Proc. Natl. Acad. Sci. U.S.A. 81*, 155–159.
Fry, D. C., Madison, V. S., Greeley, D. N., Felix, A. M., Heimer, E. P., Frohman, L., Campbell, R. M., Mowles, T. F., Toome, V., & Wegrzynski, B. B. (1992) *Biopolymers 32*, 649–666.
Ghadiri, M. R., & Fernholtz, A. K. (1990) *J. Am. Chem. Soc. 112*, 9633–9635.
Greenfield, N., & Fasman, G. D. (1969) *Biochemistry 8*, 4108–4116.
Harper, E. T., & Rose, G. D. (1993) *Biochemistry 32*, 7605–7609.
Heinrikson, R. L., & Meredith, S. C. (1984) *Anal. Biochem. 136*, 65–74.
Hussain, M. M., Maxfield, F. R., Más-Oliva, J., Tabas, I., Ji, Z.-S., Innerarity, T. L., & Mahley, R. W. (1991) *J. Biol. Chem. 266*, 13936–13940.
Innerarity, T. L., Pitas, R. E., & Mahley, R. W. (1979) *J. Biol. Chem. 254*, 4186–4190.
Innerarity, T. L., Friendlander, E. J., Rall, S. C., Jr., Weisgraber, K. H., & Mahley, R. W. (1983) *J. Biol. Chem. 258*, 12341–12347.
Jackson, D. Y., King, D. S., Chmielewski, J., Singh, S., & Schultz, P. G. (1991) *J. Am. Chem. Soc. 113*, 9391–9392.
Kaiser, E. T., & Kézdy, F. J. (1984a) *Science 259*, 249–255.
Kaiser, E. T., & Kézdy, F. J. (1984b) *Proc. Natl. Acad. Sci. U.S.A. 80*, 1137–1143.
Kaiser, E. T., & Kézdy, F. J. (1987) *Annu. Rev. Biophys. Biophys. Chem. 16*, 561–581.
Kim, P. S., & Baldwin, R. L. (1984) *Nature 307*, 329–334.
Kim, Y., & Prestegard, J. H. (1989) *J. Magn. Reson. 84*, 9–13.
Kowal, R. C., Herz, J., Goldstein, J. L., Esser, V., & Brown, M. S. (1989) *Proc. Natl. Acad. Sci. U.S.A. 86*, 5810–5814.
Kraulis, P. J., Clore, G. M., Nilges, M., Jones, T. A., Pettersson, G., Knowles, J., & Gronenborn, A. M. (1989) *Biochemistry 28*, 7241–7257.
Low, B. W., & Baybutt, R. B. (1952) *J. Am. Chem. Soc. 74*, 5806–5807.
Lyu, P. C., Wemmer, D. E., Zhou, H. X., Pinker, R. J., & Kallenbach, N. R. (1993) *Biochemistry 32*, 421–425.
Macura, S., & Ernst, R. R. (1980) *Mol. Phys. 41*, 95–117.
Mahley, R. W. (1988) *Science 240*, 622–630.
Marqusee, S., & Baldwin, R. L. (1987) *Proc. Natl. Acad. Sci. U.S.A. 84*, 8898–8902.
Matsushima, T., Getz, G. S., & Meredith, S. C. (1990) *Nucleic Acids Res. 18*, 202.
Nakagawa, Y., Gillen, M. F., & Williams, R. E. (1976) *Can. J. Chem. 54*, 3200–3202.
Nilges, M., Clore, G. M., & Gronenborn, A. M. (1988a) *FEBS Lett. 239*, 129–136.
Nilges, M., Clore, G. M., & Gronenborn, A. M. (1988b) *FEBS Lett. 229*, 317–324.
Oas, T. G., & Kim, P. S. (1988) *Nature 336*, 42–48.
Ösapay, G., & Taylor, J. W. (1992) *J. Am. Chem. Soc. 114*, 6966–6973.
Osterhout, J. J., Jr., Handel, T., Na, G., Toumadje, A., Long, R. C., Connolly, P. J., Hoch, J. C., Johnson, W. C., Jr., Live, D., & DeGrado, W. F. (1992) *J. Am. Chem. Soc. 114*, 331–337.
Otting, G., Widmer, H., Wagner, G., & Wüthrich, K. (1986) *J. Magn. Reson. 66*, 187–193.
Pauling, L., & Corey, R. B. (1950) *J. Am. Chem. Soc. 72*, 5349.
Pease, J. H., Storrs, R. W., & Wemmer, D. E. (1990) *Proc. Natl. Acad. Sci. U.S.A. 87*, 5643–5647.
Presta, L. G., & Rose, G. D. (1988) *Science 240*, 1632–1641.
Ramakrishnan, C., & Ramachandran, G. N. (1965) *Biophys. J. 5*, 909–933.
Rance, M. (1987) *J. Magn. Reson. 74*, 557–564.
Rance, M., Sørensen, O. W., Bodenhausen, G., Wagner, G., Ernst, R. R., & Wüthrich, K. (1983) *Biochem. Biophys. Res. Commun. 117*, 479–485.
Reed, J., & Kinzel, V. (1991) *Biochemistry 30*, 4521–4528.
Reed, J., & Kinzel, V. (1993) *Proc. Natl. Acad. Sci. U.S.A. 90*, 6761–6765.
Richardson, J. S., & Richardson, D. C. (1988) *Science 240*, 1648–1652.
Ruan, F., Chen, Y., & Hopkins, P. B. (1990) *J. Am. Chem. Soc. 112*, 9403–9404.
Sarin, V. K., Kent, S. B. H., Tam, J. P., & Merrifield, R. B. (1981) *Anal. Biochem. 117*, 147–157.
Serrano, L., & Fersht, A. R. (1989) *Nature 342*, 296–299.
Serrano, L., Neira, J.-L., Sancho, J., & Fersht, A. R. (1992) *Nature 356*, 453–455.
Sklenar, V., & Bax, A. (1987) *J. Magn. Reson. 74*, 469–479.
States, D. J., Haberkorn, R. A., & Ruben, D. J. (1982) *J. Magn. Reson. 48*, 286–292.
Stickle, D. F., Presta, L. G., Dill, K. A., & Rose, G. D. (1992) *J. Mol. Biol. 226*, 1143–1159.
Westerlund, J. A., & Weisgraber, K. H. (1993) *J. Biol. Chem. 268*, 15745–15750.
Willnow, T. E., Goldstein, J. L., Orth, K., Brown, M. S., & Herz, J. (1992) *J. Biol. Chem. 267*, 26172–26180.
Wilson, C., Wardell, M. R., Weisgraber, K. H., Mahley, R. W., & Agard, D. A. (1992) *Science 252*, 1817–1822.
Wüthrich, K. (1986) *NMR of Proteins and Nucleic Acids*, John Wiley and Sons, New York.
Yokoyama, S., Fukushima, D., Kupferberg, J. P., Kézdy, F. J., & Kaiser, E. T. (1980) *J. Biol. Chem. 255*, 7333–7339.
Zhou, H. X., Lyu, P. C., Wemmers, D. E., & Kallenbach, N. R. (1994) *J. Am. Chem. Soc. 116*, 1139–1140.